Three-Dimensional Quantum Transport Simulation of Si-Nanowire Transistors Based on Wigner Function Model

Yoshihiro Yamada and Hideaki Tsuchiya
Department of Electrical and Electronics Engineering
Graduate School of Engineering, Kobe University
1-1, Rokko-dai, Nada-ku, Kobe, 657-8501, Japan
065t804t@stu.kobe-u.ac.jp

Abstract—**We have developed a new self-consistent and three-dimensional quantum simulator for Si-nanowire transistors based on the Wigner function model, coupled with Schrödinger-Poisson algorithm. To achieve a sufficient accuracy for calculating subthreshold current, we introduced a third-order differencing scheme for discretizing the diffusion term in the Wigner transport equation. Then, by comparing with semiclassical Boltzmann and non-equilibrim Green's function approaches, the validity of the present simulator is discussed.**

***Index-terms*—Si-nanowire transistors, quantum transport, Wigner function, source-drain tunneling, quantum confinement**

I. INTRODUCTION

Si-nanowire transistors (SNWTs) are promising candidates as extremely downscaled MOSFETs for the future Si-VLSIs, because device structures with gate-all-around (GAA) configurations provide better electrostatic control than the conventional planar structures, and a higher current capability due to an improved electronic bandstructure is expected [1]. To understand the device physics of SNWTs and assess their performance limits, a fully quantum simulator considering electrostatic gate control, atomistic effects and realistic scattering processes is required. In this paper, we present a new self-consistent and three-dimensional quantum simulator based on a direct solution of the Wigner transport equation [2, 3], coupled with Schrödinger-Poisson algorithm. In particular, we introduced a third-order differencing scheme for discretizing the diffusion term in the Wigner transport equation, to achieve a sufficient numerical accuracy in the subthreshold region. The present quantum simulator can handle all quantum effects in SNWTs, such as two-dimensional quantum confinement and source-drain (SD) tunneling, where the significance of SD tunneling is verified by comparing with semiclassical Boltzmann approach. Furthermore, the subthreshold swings are compared with the results from the non-equilibrium Green's function (NEGF) method [4], and its validity and a scaling limit are discussed.

II. COMPUTATIONAL METHOD

A. Model and Theory

The SNWT device model used in this study is shown in Fig. 1 (a), where GAA structure is employed, and its cross-section is 3nm-square with the gate oxide thickness of 0.5nm. The doping concentration in the source and drain regions is 10^{20} cm^{-3} and the channel region is undoped. The conduction band valleys of Si is shown in Fig. 1 (b), where the channel direction is taken as <100> and the confinement directions <010> and <001>. To simulate quantum transport in such nano-MOS devices, we have developed the computational algorithm based on Wigner transport formalism as shown in Fig. 2. In this approach, the Wigner distribution function is defined for each quantized subband n for the three-pairs of the valleys, $E_n^{\nu}(x)$, which is calculated by solving the 2D Schrödinger equations for each y-z cross-section and each conduction band valley (ν = 1-1', 2-2', 3-3'). We applied the Lanczos method based on the modified Gram-Schmidt orthogonalization to solve the 2D Schrödinger equations. Then, by using the obtained subband profiles, 1D Wigner transport equation at steady state given below is solved along the source-drain direction x.

$$\frac{\hbar k}{m_v^*}\frac{\partial f^{n,\nu}}{\partial \chi}+\frac{1}{\hbar}\int\frac{dk'}{2\pi}V^{n,\nu}(\chi,k-k')f^{n,\nu}(\chi,k')=\left(\frac{\partial f}{\partial t}\right)_C \qquad (1)$$

where $V^{n,\nu}(\chi,k)$ is the non-local potential driving term given by

$$V^{n,\nu}(\chi,k)=\int_{-\infty}^{\infty}d\xi\sin(k)\left[E_n^{\nu}\left(\chi+\frac{\xi}{2}\right)-E_n^{\nu}\left(\chi-\frac{\xi}{2}\right)\right] \qquad (2)$$

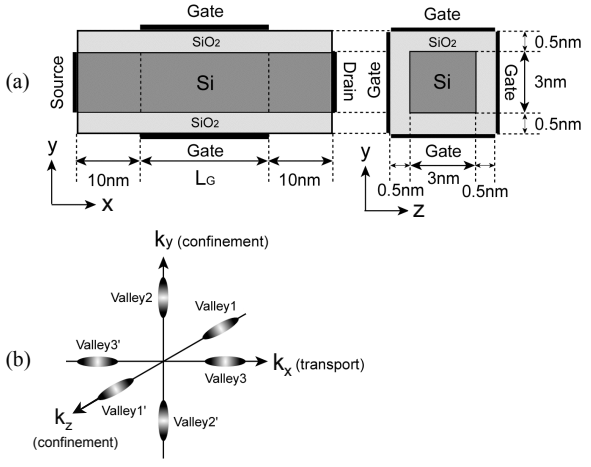

Fig. 1 (a) GAA-SNWT device model and (b) conduction band valleys of Si.

This work was supported by the Semiconductor Technology Academic Research Center (STARC).

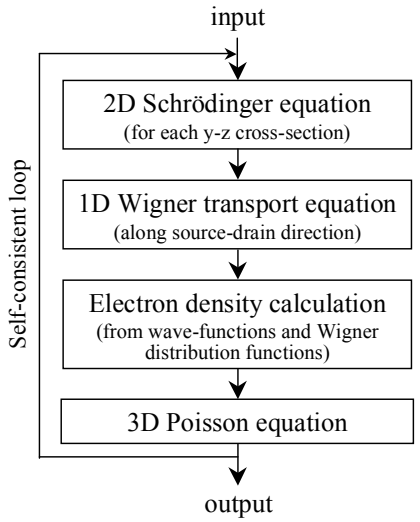

Fig. 2 Computational algorithm based on Wigner function model.

This term represents quantum mechanical effects such as tunneling. Note that χ and ξ denote the diagonal and cross-diagonal coordinates between space variables x and x' for two particles, respectively; $\chi = (x + x')/2$ and $\xi = x - x'$.

The right-hand side of eq. (1) stands for a collisional term. For phonon scatterings, the collisional term can be represented by the same integral expression as in the Boltzmann transport equation [5], which involves the distribution functions of carriers in different subbands and at different wavenumbers. In this paper, however, we employ the simpler relaxation time approximation (RTA) as a first step to consider scattering effects, which is given by [6, 7, 8]

$$\left(\frac{\partial f}{\partial t}\right)_C \approx -\frac{1}{\tau}\left[f^{n,v}(x,k_x) - \frac{f_{eq}^{n,v}(x,k_x)}{\int dk_x f_{eq}^{n,v}(x,k_x)} \int dk_x' f^{n,v}(x,k_x') \right] \quad (3)$$

where τ and $f_{eq}^{n,v}$ denote the relaxation time and the distribution functions at equilibrium ($V = 0$), respectively, and eq. (3) ensures charge conservation. Here, $f_{eq}^{n,v}$ was substituted by the equilibrium Wigner distribution functions computed at $V_D = 0$V. The value of τ was calculated from the mobility of 500 cm^2 / (V · s) by $\tau_v = m_v^* \mu / e$ for each conduction band valley, since the mobility is a more familiar parameter than the relaxation time.

To analyze the gate control in SNWTs, the 3D Poisson equation is self-consistently solved by using the preconditioned conjugate gradient method with the incomplete Cholesky factorization. Since the main purpose of this study is to demonstrate the validity of the present Wigner approach, we introduced the effective mass approximation and RTA. However, the present approach is applicable for atomistic simulation beyond the effective mass approximation and can include physics-based scattering processes [5]. Such extensions are currently in progress.

B. Discretization Method

As is well known, numerical solutions of the Wigner function model significantly depend on discretization methods for solving eqs. (1) and (2). Frensley pointed out that discrete Wigner function is not generally consistent with discrete density operator, and thus some of the information contained in the density operator will be lost in the Wigner function, because the (χ, ξ) mesh points are only half as dense as the (x, x') mesh points [6]. A way to incorporate all the (x, x') points might be to use a staggered mesh in (χ, ξ) with mesh spacing of $\Delta_\chi = (1/2)\Delta_x$ and $\Delta_\xi = 2\Delta_x$. Mains and Haddad have investigated such a scheme on the potential driving term of eq. (2), but it seems to be only applicable for equilibrium situation due to the requirement for central differencing scheme (CDS) to be employed [9]. Therefore, we adopted here higher-order accurate discretizations for the spatial derivative term on the left-hand side of eq. (1) [7]. We expect that such a simpler modification will be effective in the present nano-MOS simulation.

In this paper, we examined three types of differencing schemes, which are upwind differencing scheme (UDS),

$$\left.\frac{\partial f}{\partial \chi}\right|_{\mathrm{UDS}} = \frac{f(\chi + \Delta_\chi) - f(\chi)}{\Delta_\chi}, \quad k < 0 \quad (4)$$

second-order upwind differencing scheme (SDS),

$$\left.\frac{\partial f}{\partial \chi}\right|_{\mathrm{SDS}} = \frac{-3f(\chi) + 4f(\chi + \Delta_\chi) - f(\chi + 2\Delta_\chi)}{2\Delta_\chi}, \quad k < 0 \quad (5)$$

and third-order upwind differencing scheme (TDS).

$$\left.\frac{\partial f}{\partial \chi}\right|_{\mathrm{TDS}} = \frac{-2f(\chi - \Delta_\chi) - 3f(\chi) + 6f(\chi + \Delta_\chi) - f(\chi + 2\Delta_\chi)}{6\Delta_\chi}, \quad k < 0 \quad (6)$$

It can be readily proven that TDS corresponds to a hybrid scheme consisting of CDS and SDS with a combination ratio of 2:1 as follows.

$$\left.\frac{\partial f}{\partial \chi}\right|_{\mathrm{TDS}} = \frac{2}{3}\frac{f(\chi + \Delta_\chi) - f(\chi - \Delta_\chi)}{2\Delta_\chi} \ (\mathrm{CDS}) + \frac{1}{3}\frac{-3f(\chi) + 4f(\chi + \Delta_\chi) - f(\chi + 2\Delta_\chi)}{2\Delta_\chi} \ (\mathrm{SDS}) \quad (7)$$

Thus, TDS may be possibly linked to the Mains and Haddad's idea mentioned above, which is worthy of consideration for

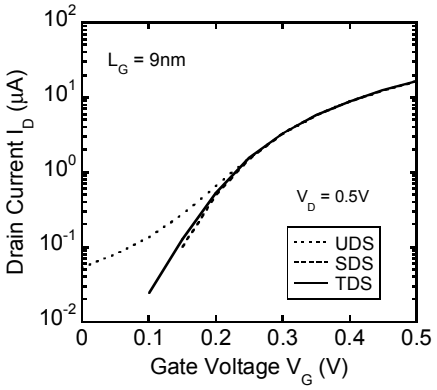

Fig. 3 I_D - V_G characteristics computed by using UDS, SDS and TDS for the spatial derivative term in the Wigner transport equation.

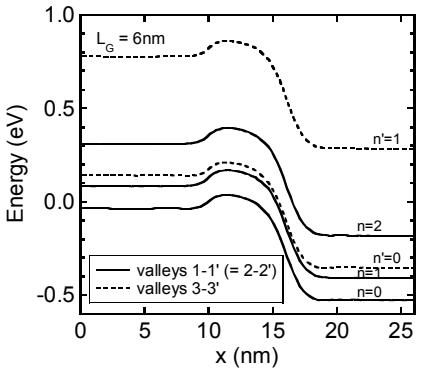

(a)

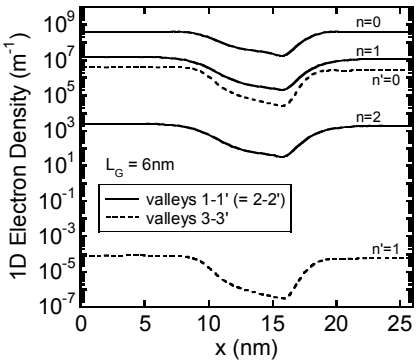

(b)

Fig. 4 (a) Subband profiles and (b) electron density profiles for several quantized subbands along source-drain direction. The channel length is 6nm, and V_D = 0.5V and V_G = 0.25V.

further improvement in numerical accuracy and stability of the Wigner function model.

The conventional boundary conditions for the Wigner transport equation [2] are used in the simulation, that is, the equilibrium Fermi-Dirac distribution functions are imposed only for the injected electrons into a device region, while distribution functions for the outgoing electrons are determined by solutions of eq. (1). Such boundary conditions should be used at the source/drain contacts sufficiently away from a quantum region, because electron transport in reservoirs attached to the device region is supposed to be classical.

III. RESULTS

A. Higher-Order Differencing Schemes

First, Fig. 3 shows the I_D - V_G characteristics computed by applying UDS, SDS and TDS to the whole device region. First, for the UDS approach, unexpectedly large subthreshold current is observed below V_G=0.2V. SDS significantly improves such a subthreshold current behavior, but it occasionally outputs negative subthreshold current at small gate biases. TDS further improves the subthreshold current behavior and allows us to estimate the subthreshold swings as presented later. On the other hand, the on-currents at large V_G conditions are almost independent of the differencing schemes. So, careful treatment

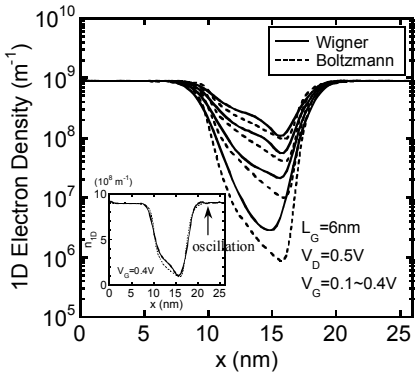

Fig. 5 Variations in total electron density profiles due to gate bias voltage. Results from a semiclassical Botzmann approach are also plotted in the dashed lines. The inset shows linear plot of the density profile at V_G = 0.4V

of differencing scheme is found to be needed for a precise simulation in the subthreshold region. Hereafter, we will use TDS in the Wigner approach.

B. Multisubband Quantum Transport

Next, we present the electrical characteristics of SNWTs. Fig. 4 shows (a) the subband profiles and (b) the electron density profiles for several quantized subbands along the source-drain direction, where L_G = 6nm, V_D = 0.5V and V_G = 0.25V. The valleys 1, 1', 2 and 2' are completely degenerated because of the square cross-section. These four valleys have the larger confinement effective mass (m_l) in the y or z direction, so their lowest (n = 0) and first higher (n = 1) subbands are located below the lowest subband of the valleys 3 and 3' (n'=0), as shown in Fig. 4 (a). As a result, most of the electrons are populated in those four valleys (1, 1', 2, 2') as shown in Fig. 4 (b). This is favorable from the point of view of drive current, because they have the smaller transport effective mass of m_t.

Next, Fig. 5 shows the variations in the total electron density profiles due to gate bias voltage. Note that each profile is compared with that from a semiclassical Boltzmann approach where the 1D Boltzmann transport equation is solved along the source-drain direction, while the 2D Schrödinger equations are solved in the same manner as mentioned in Sec. II-*A*. It is found that the electron densities inside the channel are larger for the Wigner approach, especially at smaller gate biases. This is due to SD tunneling discussed later again. In addition, the inset in Fig. 5 shows the linear plot of the density

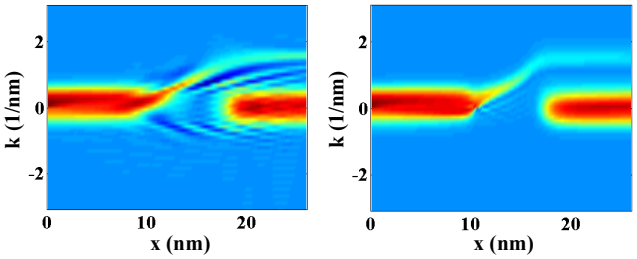

(a) (b)

Fig. 6 (a) Wigner and (b) Boltzmann distribution functions. L_G = 6nm, V_D = 0.5V and V_G = 0.4V.

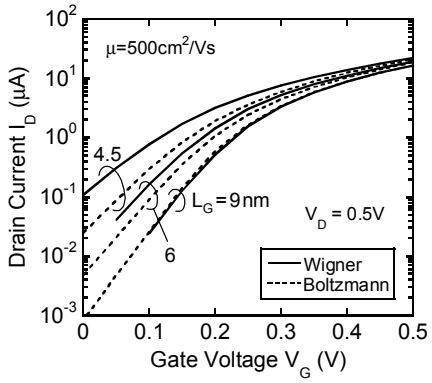

Fig. 7 I_D-V_G characteristics for L_G = 9nm, 6nm and 4.5nm, computed by using the Wigner and Boltzmann approaches.

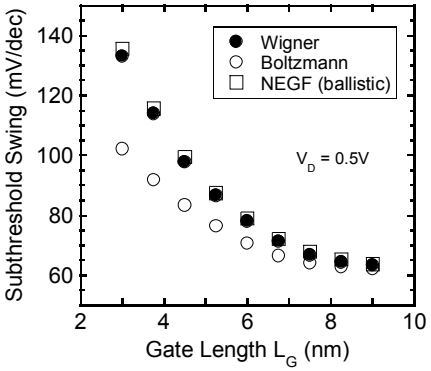

Fig. 8 Gate length dependences of subthreshold swings computed by using the Wigner, Boltzmann and ballistic NEGF approaches.

profile at V_G = 0.4V, which indicates a weak oscillation in the drain region for the Wigner function model. This is caused by an interference effect between right-going and left-going electron waves, which is emphasized by hot electrons in the drain region as shown in Fig. 6 (a). Please take notice that the interference pattern still exists at the right boundary. This suggests that a longer drain region or phase randomizing process should be introduced, to be consistent with the boundary conditions described in Sec. II-*B*.

Fig. 7 shows the I_D-V_G characteristics for L_G = 9nm, 6nm and 4.5nm, computed by using the Wigner and Boltzmann approaches. In the Wigner approach, a perceptible increase of the subthreshold current is obtained for the channels shorter than 6nm [10], which is due to SD tunneling as mentioned above. On the other hand, at high V_G conditions, the two approaches become closer because thermal injection is a dominant carrier injection process at the on-state. Furthermore, the subthreshold swings (SS) are compared with the results from the ballistic NEGF method as shown in Fig. 8, where we also developed the NEGF program in this study. It is remarkable that the Wigner and ballistic NEGF results coincide closely for a wide range of gate length shorter than 10nm, which means that scatterings have a very small impact in the subthreshold region and also that SD tunneling is adequately simulated in the Wigner function model. Incidentally, it has been demonstrated that SS values are barely affected by scattering effects within RTA based on the semiclassical Boltzmann approach [11], and in this study we verified that it is true even when SD tunneling is incorporated by the Wigner approach. Therefore, the comparison with the ballistic NEGF method in the subthreshold region is reasonable. Further, from Fig. 8 the semiclassical simulation without SD tunneling (Boltzmann) might predict about 1nm shorter minimum gate length enabling us to make electrostatically "well-tempered" GAA-SNWTs with a SS less than 80mV/dec [12]. This discrepancy will be not negligible in practical design of SNWTs with sub-10nm channel length.

At Present, the Wigner approach can not provide electrical characteristics around V_G=0V for the longer channel devices as found in Fig. 7. This is considered due to the lack of numerical accuracy under the high potential barrier situations. Thus, we need to develop more advanced computational techniques, such as more accurate discretization method and a proper connection with the boundary conditions, for reliable off-current estimation.

IV. Conclusion

We have developed a three-dimensional quantum simulator for SNWTs based on the Wigner function model, which can consider electrostatic gate control, two-dimensional quantum confinement and SD tunneling in GAA-SNWTs. Its validity was confirmed by the comparison with the semiclassical Boltzmann and NEGF approaches. As a result, SD tunneling can be a critical physical phenomenon related to a scaling limit of nanowire devices. We further pointed out that some advancements in the computational techniques are required to apply the Wigner function model to the off-current analysis.

Acknowledgment

This work was supported by the Semiconductor Technology Academic Research Center (STARC).

References

[1] N. Neophytou, A. Paul, M. Lundstrom, and G. Klimeck, *IEEE Trans. Electron Devices*, **55** (2008) 1286.

[2] W. R. Frensley, *Phys. Rev. B*, **36** (1987) 1570.

[3] H. Tsuchiya, M. Ogawa, and T. Miyoshi, *IEEE Trans. Electron Devices*, **38** (1991) 1246.

[4] S. Datta, *Electronic Transport in Mesoscopic Systems*, Cambridge, U. K.: Cambridge University Press, 1995.

[5] H. Tsuchiya and T. Miyoshi, *J. Appl. Phys.*, **83** (1998) 2574.

[6] W. R. Frensley, *Rev. Mod. Phys.*, **62** (1990) 745.

[7] F. A. Buot and K. L. Jensen, *Phys. Rev. B*, **42** (1990) 9429.

[8] H. Tsuchiya, M. Ogawa, and T. Miyoshi, *IEEE Trans. Electron Devices*, **39** (1992) 2465.

[9] R. K. Mains and G. I. Haddad, *J. Comput. Phys.*, **112** (1994) 149.

[10] D. Querlioz, J. S.-Martin, K. Huet, A. Bournel, V. A.-Fortuna, C. Chassat, S. G.-Retailleau, and P. Dollfus, *IEEE Trans. Electron Devices*, **54** (2007) 2232.

[11] S. Scaldaferri, G. Curatola, and G. Iannaccone, *IEEE Trans. Electron Devices*, **54** (2007) 2901.

[12] S. Jin, T. W.-Tang, and M. V. Fischetti, *IEEE Trans. Electron Devices*, **55** (2008) 727.